ELSEVIER

Structural analysis of gradient elastic components

A.E. Giannakopoulos *, K. Stamoulis

Laboratory for Strength of Materials and Micromechanics, Department of Civil Engineering, University of Thessaly, Volos 38336, Greece

Abstract

The present study investigates the size effects in the problems of cantilever beam bending and cracked bar tension within the gradient elasticity framework. Analytical solutions for metrics that characterize both the normalized stiffness and toughness are derived. It is found that the gradient elastic beam exhibits a significantly stiffer but also more brittle response, while the gradient cracked bar exhibits considerable toughening. These results compare well with respective finite element computations.
© 2006 Elsevier Ltd. All rights reserved.

Keywords: Gradient elasticity; Microstructural lengths; Size effects; Micro-electromechanical systems (MEMS); Structural analysis; Bending stiffness; Toughness; Fatigue

1. Introduction

The dimensions of structures and systems in engineering are scaled down to the micro- (e.g., thin films, micro-electromechanical systems (MEMS)) and nano-domains (e.g., nano-electromechanical systems (NEMS)). In many current practical applications of MEMS, typical structural components are in the form of beams, bars, plates and membranes (e.g., sensors and actuators) and deform elastically (Senturia, 2001). In such small-scale structures, the material microstructural length scales become comparable to the length scale of the deformation field and the mechanical behavior becomes non-homogeneous and size-dependent. Nevertheless, there have been several studies as well as experimental evidence directed to elastic solids of much larger scales which also exhibit size-dependent behaviors (e.g., see Kakunai et al., 1985 for polycrystalline aluminum beams bending, and Anderson and Lakes, 1994 for beam bending and rod torsion in closed-cell foams). Classical elasticity theory is not adequate in capturing any size effect, since it possesses no characteristic length (i.e., material parameter with length dimension) in the governing equations. Thus, one has to resort to higher-order continuum theories (micropolar, couple-stress and strain gradient elasticity (SGE) theories), which take into account the effect of microstructure by including explicit material length scales in their structure. A major obstacle to the usage of the aforementioned higher-order models is the complexity of the general

---

* Corresponding author. Tel.: +30 24210 74179; fax: +30 24210 74169.
  E-mail address: agiannak@uth.gr (A.E. Giannakopoulos).

theories involved (e.g., Cosserat and Cosserat, 1909; Koiter, 1964; Mindlin, 1964; Eringen, 1966). The use of simpler, engineering-type gradient theories (e.g., Vardoulakis and Sulem, 1995; Papargyri-Beskou et al., 2003) is much more convenient as well as valid, as was recently shown by Giannakopoulos et al. (2006).

In the current study, we investigate analytically the microstructural size effects in the problems of cantilever beam bending and cracked bar uniaxial tension with the use of a simple, yet rigorous SGE theory. The employed framework follows the general concept and structure of Mindlin's theory, nevertheless is associated with only three material constants (two classical and one non-classical) instead of the 18, 6 or even 4 elastic constants of the more general theories of Mindlin (1964), Eringen (1966) or Koiter (1964), respectively. The application of all possible boundary conditions is discussed with the aid of respective finite element computations (Giannakopoulos et al., 2006) which compare well with the analytical results. The bending of cantilever beam is also considered in a recent paper (Lam et al., 2003) on the basis of a new SGE theory. This framework also follows Mindlin's simplified formulation, but requires an additional equilibrium condition to govern the behavior of higher-order stresses, the equilibrium of moments of couples (Lam et al., 2003).

Furthermore, a procedure introduced by Kienzler and Herrmann (1986) and based on the principle of virtual work, is employed in order to compute the strain energy release rate of the cracked bar under tension. The study concludes with the assessment of the gradient-elasticity effect on both the normalized stiffness and toughness of the structural components under discussion. The microstructural length of the current modeling is calculated by applying the analytical results for the normalized stiffness of a cantilever beam to respective experimental results of Kakunai et al. (1985). This length exhibits a stronger correlation to the grain size as compared to the length calculated by Kakunai et al. with reference to Koiter's theory (Koiter, 1964).

2. Bending of a gradient elastic cantilever beam

2.1. A review of the employed strain gradient elasticity framework

We consider a cantilever, Bernoulli–Euler beam of length L and thickness H with its built-in end at $x = 0$, subjected to a lateral load $\overline{P}$ at its free end, as illustrated schematically in Fig. 1. On the basis of the employed theory (form II SGE in Mindlin, 1964) and with respect to the one-dimensional case of beam bending, the constitutive equations for the Cauchy, double and total stresses τ_x, μ_x and σ_x, respectively, are given by:

$$\tau_x = E\varepsilon_x, \quad \mu_x = g^2 E\varepsilon_x', \quad \sigma_x = \tau_x - \frac{\mathrm{d}\mu_x}{\mathrm{d}x} = E(\varepsilon_x - g^2 \varepsilon_x'') \tag{1}$$

where ε_x represents the axial strain of the beam in bending, E is the Young's modulus, g represents a material microstructural length and primes indicate differentiation with respect to x. In this case, σ_x is also the true traction on the cross-section of the beam. Moreover, according to Bernoulli–Euler hypothesis, the axial strain, ε_x is given by:

$$\varepsilon_x = -\frac{\mathrm{d}^2 u}{\mathrm{d}x^2} y \tag{2}$$

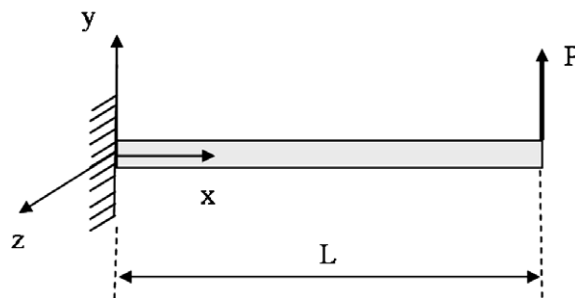where u represents the y-deflection of the beam in bending.

Fig. 1. Configuration and loading of the beam under consideration. Note that $\overline{P}$ denotes the applied load P per unit of out-of-plane thickness ($\overline{P} = P$).

Utilizing Eq. (2) and conditions of equilibrium, the governing equation of a beam in bending takes the form (Papargyri-Beskou et al., 2003):

$$EI(u^{\mathrm{IV}} - g^2 u^{\mathrm{VI}}) = 0 \tag{3}$$

where I is the moment of inertia about the z-axis.

Finally, the corresponding boundary conditions determined by means of a variational principle (Papargyri-Beskou et al., 2003) satisfy the equations:

$$[V(L) - EI[u'''(L) - g^2 u^{\mathrm{V}}(L)]]\delta u(L) - [V(0) - EI[u'''(0) - g^2 u^{\mathrm{V}}(0)]]\delta u(0) = 0$$
$$[M(L) - EI[u''(L) - g^2 u^{\mathrm{IV}}(L)]]\delta u'(L) - [M(0) - EI[u''(0) - g^2 u^{\mathrm{IV}}(0)]]\delta u'(0) = 0 \tag{4}$$
$$[m(L) - EI[g^2 u'''(L)]]\delta u''(L) - [m(0) - EI[g^2 u'''(0)]]\delta u''(0) = 0$$

where V represents the boundary shear force and M, m are the boundary classical and non-classical (double) bending moments, respectively. Note that Eq. (4) defines complementary the dynamic and the kinematic boundary conditions.

2.2. Solution for the boundary value problem

Next, we solve the boundary value problem for the configuration and loading indicated in Fig. 1. The governing equation given by Eq. (3) has a general solution of the form:

$$u(x) = c_1 x^3 + c_2 x^2 + c_3 x + c_4 + c_5 g^4 \sinh\left(\frac{x}{g}\right) + c_6 g^4 \cosh\left(\frac{x}{g}\right) \tag{5}$$

The classical boundary conditions are

$$u(0) = u'(0) = 0, \quad M(0) = \overline{P}L, \quad M(L) = 0 \tag{6}$$

and the non-classical boundary conditions are assumed to be

$$u''(0) = u'''(L) = 0 \tag{7}$$

The latter condition $u'''(L) = 0$ implies no double bending moment at the free end $[m(L) = 0]$, whereas the former condition $u''(0) = 0$ implies that we want the beam to obtain maximum stiffness without enforcing $m(0)$.

The use of the above boundary conditions enables us to determine the constants c_1 through c_6 of the Eq. (5), which yields the deflection as:

$$u(x) = \left(-\frac{\overline{P}}{6EI}\right)x^3 + \left(\frac{\overline{P}L}{2EI}\right)x^2 + \left[-\frac{\overline{P}g^2}{EI}\frac{1}{\cosh(L/g)} - \frac{\overline{P}Lg}{EI}\tanh\left(\frac{L}{g}\right)\right]x$$
$$+ \left[\frac{\overline{P}g^3}{EI}\frac{1}{\cosh(L/g)} + \frac{\overline{P}Lg^2}{EI}\tanh\left(\frac{L}{g}\right)\right]\sinh\left(\frac{x}{g}\right) + \left(-\frac{\overline{P}Lg^2}{EI}\right)\cosh\left(\frac{x}{g}\right) + \frac{\overline{P}Lg^2}{EI} \tag{8}$$

2.3. Stiffness metrics for the gradient elastic beam

Using the solution of Eq. (8), we compute the deflection at the free end of the gradient beam to be

$$u(x = L) = \frac{\overline{P}L^3}{3EI}\left\{1 - 3\left(\frac{g}{L}\right)^2\left[\cosh\left(\frac{L}{g}\right) + \frac{1}{\cosh(L/g)} + \left(\frac{L}{g}\right)\tanh\left(\frac{L}{g}\right) - 1\right]\right\}$$
$$+ \frac{\overline{P}L^3}{3EI}\left\{3\left(\frac{g}{L}\right)^3\left[\tanh\left(\frac{L}{g}\right) + \left(\frac{L}{g}\right)\sinh\left(\frac{L}{g}\right)\tanh\left(\frac{L}{g}\right)\right]\right\} \tag{9}$$

Note that Eq. (9) predicts the classical elasticity result, u_c in the limit $g \to 0$

$$u_c = u(x = L, g = 0) = \frac{\overline{P}L^3}{3EI} \tag{10}$$

Now, the normalized deflection, u/u_c is plotted as a function of the non-dimensional parameter, g/L (micro-structural length over beam length) in Fig. 2. This plot shows that the normalized deflection is decreasing monotonically with g/L, predicting a considerably stiffer response for the gradient beam as compared to the classical theory prediction.

The numerical evaluation for small values of the non-dimensional parameter g/L ($0 \leqslant g/L < 0.025$) shows oscillations between infinity and zero which are not real. Therefore, we performed an asymptotic analysis which, after extensive calculation, shows that

$$\lim_{g/L \to 0} u/u_c = 1, \quad \lim_{g/L \to 0} \frac{\partial(u/u_c)}{\partial(g/L)} = -3 \tag{11}$$

Thus, the normalized deflection function for small values of g/L is very well approximated by the linear form

$$u/u_c = 1 - 3(g/L) \tag{12}$$

Next, the maximum strain distribution along the x-axis, $\overline{\varepsilon_x}$ as a function of the non-dimensional distance, x/L, and the non-dimensional parameter, g/L, is derived from Eqs. (2) and (9) to be

$$\overline{\varepsilon_x}(x) = \varepsilon_o \left\{ 1 - \left(\frac{x}{L}\right) - \cosh\left(\frac{x/L}{g/L}\right) + \left[\frac{g/L}{\cosh(L/g)} + \tanh\left(\frac{L}{g}\right)\right] \sinh\left(\frac{x/L}{g/L}\right) \right\} \tag{13}$$

where for an orthogonal cross-section with height H, the maximum strain, ε_o, is given by

$$\varepsilon_o = \frac{6\overline{P}L}{EH^2} \tag{14}$$

Note that for beams with other than orthogonal type of cross-sections, ε_o takes appropriate form in accord to the classical beam analysis.

The plot in Fig. 3 shows the variation of the normalized strain distribution along the x-axis, $\overline{\varepsilon_x}/\varepsilon_o$ for various values of the non-dimensional parameter, g/L. The single dashed line is referred to the classical elasticity solution which Eq. (13) predicts in the limiting case of $g/L \to 0$. It is apparent that $\overline{\varepsilon_x}/\varepsilon_o$ decreases very fast as g/L increases from 0 to 1, reaffirming a stiffer response for the gradient case as compared to the classical case. Also, a very interesting observation is that the maximum strain for the gradient case does not correspond to the fixed end of the cantilever beam as it happens in the classical case. The implication of the reduction of the maximum tensile strain for the fatigue life predictions will be discussed later.
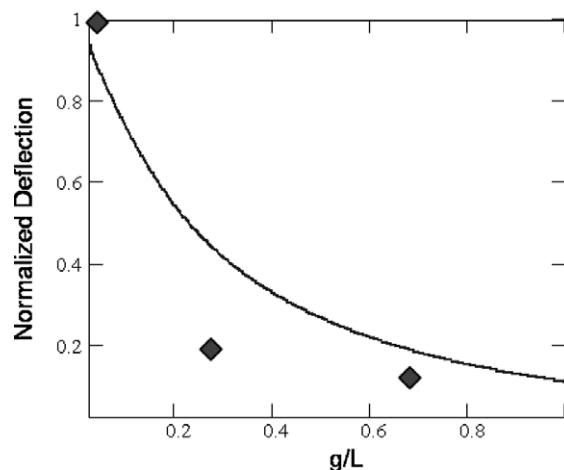

Fig. 2. Dependence of normalized deflection u/u_c, at the free end of beam on g/L (microstructural length over beam length). The diamond symbols show the predictions of a two-dimensional finite element model (see Giannakopoulos et al., 2006).
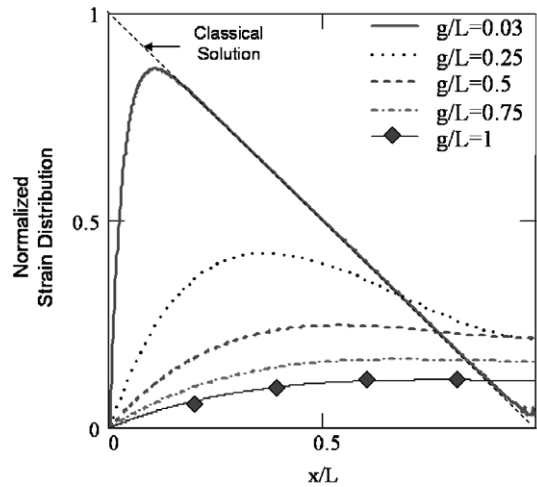
Fig. 3. Dependence of the normalized strain distribution along x-axis, $\bar{\varepsilon}_x/\varepsilon_o$ on g/L (microstructural length over beam length).

As noted in the introduction, Lam et al. (2003) have also addressed recently the bending of cantilever beam on the basis of a new SGE theory which follows Mindlin's simplified formulation, nevertheless requires additionally the equilibrium of moments of couples. Furthermore, this analysis, while also indicating significant size effect and stiffer response in bending of gradient cantilever beam, does not result in stiffness metrics comparable to the present. Specifically, a power series expansion in terms of the beam thickness is used to simplify the differential equations and boundary conditions resulting in a different set of deformation measures dependent on the beam's thickness. The specific expansion in terms of the beam thickness gives results similar to Koiter's (1964), where the stiffness increases due to the smallness of the beam thickness.

2.4. Discussion about the non-classical boundary conditions

The solution of the boundary value problem presented in Section 2.2 of the current article is determined on the basis of the assumption of the non-classical boundary conditions (see Eq. (7)).

It is apparent from the plot of Fig. 3 that the selection of $u''(0) = 0$ as a boundary condition results in the development of a boundary layer near the fixed end of the cantilever beam (Aravas, 2005). Therefore, possible alternative boundary conditions for that end of the beam have been examined. Specifically, when alternative boundary conditions for $u''(0)$ or $u'''(0)$ and $u^{IV}(0)$ were assumed, either the gradient stiffness metrics increase with g/L or they decrease, however, with a significant deviation from the finite elements results of the two-dimensional model (see Giannakopoulos et al., 2006) which compare well with the results presented in Sections 2.2 and 2.3.

2.5. Experimental assessment of gradient stiffness metrics

Experimental data of heterodyne holographic interferometry obtained by Kakunai et al. (1985) have been used to calculate the characteristic microstructural length of the present modeling (see Appendix A for details of this calculation). The plot in Fig. 4 indicates that the length g calculated with reference to the current modeling exhibits a stronger correlation to grain size d as compared to the length l calculated by Kakunai et al. with reference to Koiter's analytical results. In the present approach, as well as in Kakunai et al. approach, the same experimental data for the bending deformation of polycrystalline aluminum beams were used. More specifically, the Koiter (couple-stress) approach predicts that "the order of magnitude of l is about one fifth of the grain size, d" (the ratio of l/d is 1/5) while the current (strain gradient) approach predicts a microstructural length g of order of magnitude of the grain size d (the range of the ratio g/d is between 1/2 and 1). According to Kakunai et al., as well as other researchers (e.g., Yang and Lakes, 1982) in "such materials with microstruc-
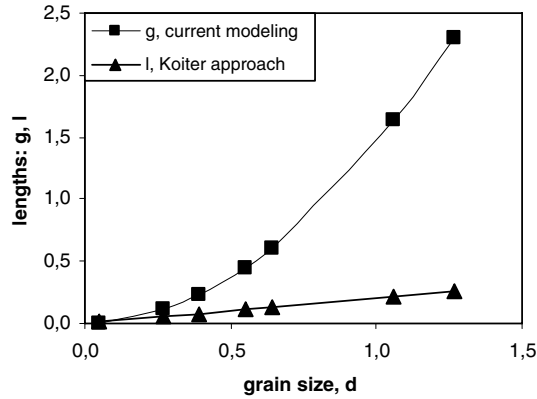
Fig. 4. Correlation of microstructural lengths to grain size of polycrystalline aluminum.

ture, the predicted characteristic length is generally as large as – or a little smaller than – the order of the size of the structural elements'' (which is the order of the grain size in our case).

Therefore, the above assessment suggests that the current modeling seems to be more successful in predicting the size effect dependence in the bending stiffness of gradient cantilever beams.

2.6. Toughness metric for the gradient elastic double cantilever beam

Next, we consider a double cantilever beam (DCB) consisting of two beams with the configuration and loading, as considered in Section 2.1 and illustrated schematically in Fig. 1. The strain energy of a beam in bending is given by (Papargyri-Beskou et al., 2003):

$$U = \frac{1}{2} \int_0^L EI[(u'')^2 + g^2(u''')^2] \mathrm{d}x \tag{15}$$

Then, taking the crack length to be the length of the beam L, the strain energy release rate of the DCB under consideration is obtained by:

$$G = \frac{\mathrm{d}(2U)}{\mathrm{d}L} \tag{16}$$

Using the solution of Eq. (8) to evaluate u'' and u''' and then substituting Eq. (15) into Eq. (16), one obtains the following expression for the strain energy release rate of the DCB:

$$
\begin{aligned}
G = {} & \frac{\overline{P^2}L^2}{EI}\left\{ 1 + \left(\frac{g}{L}\right)^2 + 2\cosh\left(\frac{L}{g}\right)\sinh\left(\frac{L}{g}\right)\left[\left(\frac{g}{L}\right) - 2c_1(x) + xc_1^2(x)\right] \right\} \\
& + \frac{\overline{P^2}L^2}{EI}\left\{ \left[\sinh^2\left(\frac{L}{g}\right) + \cosh^2\left(\frac{L}{g}\right)\right][1 + c_1^2(x)] - 4xc_1(x)\sinh^2\left(\frac{L}{g}\right) \right\} \\
& + \frac{\overline{P^2}L^2}{EI}\left\{ \left[2\tanh\left(\frac{L}{g}\right)\left[c_1(x) - \tanh\left(\frac{L}{g}\right)\right]\right]\left[1 - \sinh\left(\frac{L}{g}\right)\right] \right\}
\end{aligned}
\tag{17}
$$

where

$$c_1(x) = \frac{x + \sinh\left(\frac{L}{g}\right)}{\cosh\left(\frac{L}{g}\right)}$$

Note that Eq. (17) predicts the classical elasticity result G_c in the limit $g \to 0$
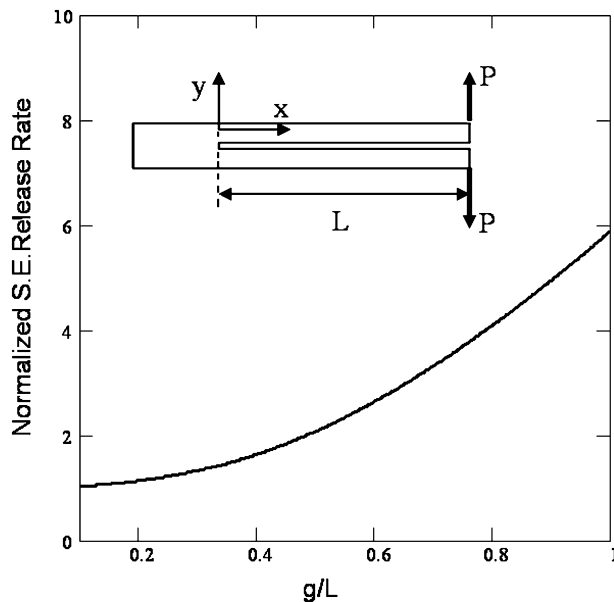
Fig. 5. Dependence of the normalized strain energy release rate, G/G_c of the gradient double cantilever beam on g/L (microstructural length over beam length). Note that $\overline{P}$ denotes the applied load P per unit of out-of-plane thickness ($\overline{P} = P$).

$$G_c = G(g = 0) = \frac{\overline{P^2}L^2}{EI} \tag{18}$$

The normalized strain energy release rate G/G_c is plotted as a function of the non-dimensional parameter g/L in Fig. 5. This plot shows that the normalized strain energy release rate is increasing monotonically with g/L, predicting a more brittle response for the gradient DCB, as compared to the classic theory prediction. This deviation becomes significant for $g/L > 0.25$. The embrittlement mechanism suggested by the DCB configuration comes as an unexpected result, contrary to the common perception that strain gradient theories predict higher strength for small structural components. Therefore, we decided to investigate an alternative cracked configuration. Next section discusses the energy release rate of a gradient elastic cracked bar in uniaxial tension.

3. Uniaxial tension of a gradient elastic cracked bar

3.1. An application of Hermann's procedure on bars with cracks

We consider a straight prismatic bar of length $2L$ and cross-sectional area A, subjected to axial tensile forces $N = A\sigma$ (where σ is the true uniaxial tensile stress) resulting in a displacement $u(x)$ along its longitudinal axis x. Furthermore, we assume a discontinuity of the bar's cross-sectional area, at $x = 0$, caused by either a central crack or two symmetrical edge cracks, which reduce the cross-sectional area to A^*, as illustrated schematically in Fig. 6.

On the basis of the employed theory (form II SGE in Mindlin, 1964), the constitutive relations are given by Eqs. (1). Furthermore, static equilibrium condition requires that

$$\frac{\partial A\sigma}{\partial x} + q = 0 \tag{19}$$

where $q = q(x)$ is the distributed axial (body) force.

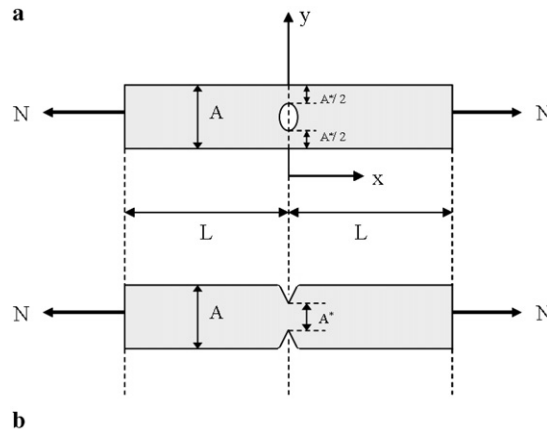Using Eqs. (1), Eq. (19) takes the form

Fig. 6. Configuration of the cracked bar under consideration: (a) with a central crack and (b) with two symmetrical edge cracks.

$$\frac{\partial A\tau}{\partial x} - \frac{\partial^2 A\mu}{\partial x^2} + q = 0 \tag{20}$$

Now, the strain energy density (per unit length) W is given by (Tsepoura et al., 2002):

$$W = \frac{1}{2} AE[(u')^2 + g^2(u'')^2] \tag{21}$$

Also, the potential of the distributed forces V is given by

$$V = -qu \tag{22}$$

Georgiadis and Grentzelou (2006) proved that the energy release rate is identical to a path-independent integral similar to the well known J-integral of Rice (1968). Now, particularizing the suggested J-integral of Georgiadis and Grentzelou and following the procedure introduced by Kienzler and Herrmann (1986), we construct two energy expressions that they are like a material force and a material load, respectively. Differentiating Eqs. (21) and (22) with respect to x, we obtain

$$W' = \frac{1}{2}(AE)'[(u')^2 + g^2(u'')^2] + AE[u'u'' + gu''(gu'')'] \tag{23}$$

$$V' = -(q'u + qu') \tag{24}$$

Substituting Eq. (20) into Eqs. (23) and (24) and after some rearrangements, we obtain

$$W' + V' - (A\tau u')' - (A\mu u'')' + [(A\mu)'u']' - \frac{1}{2}(AE)'[(u')^2 + g^2(u'')^2] + q'u - AEgg'(u'')^2 = 0 \tag{25}$$

Note that in the present formulation, we allow the cross-section A and the material properties E,g to be functions of x. Obviously, in the simplest case they are constants ($A' = 0, E' = 0, g' = 0$).

Now, we define a material force B and a material load b according to Eshelby's energy-momentum tensor (Eshelby, 1975), as follows:

$$B = W + V - A\tau u' - A\mu u'' + (A\mu)'u' \tag{26}$$

$$b = -\frac{1}{2}(AE)'[(u')^2 + g^2(u'')^2] + q'u - AEgg'(u'')^2 \tag{27}$$

Therefore, Eq. (25) may be rewritten as

$$B' = -b \tag{28}$$

Finally, using B', we define a momentum term which is equivalent to the energy release rate G, by evaluating B' at the region of discontinuity (exactly at the cracked region), where $b = 0$. This leads to the following jump condition

$$G = 2[\![B]\!] = 2[B(x = 0^+) - B(x = 0^-)] \tag{29}$$

3.2. Solution for a characteristic boundary value problem

Next, we will examine the problem where the gradient cracked bar has uniform cross-section A and homogeneous material properties E, g and is subjected to a given axial tensile force $N = P_o$ only at its free ends. Assuming zero body forces ($q = 0$, thus $V = 0$), the governing equation of the bar is given by (Tsepoura et al., 2002):

$$u''(x) - g^2 u^{IV}(x) = 0 \tag{30}$$

and has a general solution of the form:

$$u(x) = c_1 e^{x/g} + c_2 e^{-x/g} + c_3 x + c_4 \tag{31}$$

For the particular problem, the classical boundary conditions are

$$u(0) = 0, \quad AE[u'(L) - g^2 u'''(L)] = P_o \tag{32}$$

where the former condition $u(0) = 0$ implies symmetric deformation with respect to x and the latter condition is about the true axial tensile force. The non-classical boundary conditions are assumed to be

$$R(L) = AEg^2 u''(L) = 0, \quad u'(0) = \varepsilon_o \tag{33}$$

where the former condition $R(L) = 0$ implies no axial double force at the free end and the latter condition $u'(0) = \varepsilon_o$ implies an increased strain, exactly at the cracked region ($\varepsilon_o \geqslant P_o/AE$), for increasing values of A/A^*.

The use of the above boundary conditions enables us to determine the constants c_1 through c_4 of the Eq. (31). They are

$$
\begin{aligned}
c_1 &= \frac{g e^{-L/g} \left(\varepsilon_o - \frac{P_o}{AE}\right)}{2 \cosh(L/g)} \\
c_2 &= -c_1 e^{2L/g} \\
c_3 &= \frac{P_o}{AE} \\
c_4 &= g\left(\varepsilon_o - \frac{P_o}{AE}\right) \tanh(L/g)
\end{aligned}
\tag{34}
$$

3.3. Toughness metric for the gradient elastic cracked bar

Next, using the general solution of Eq. (31), we compute u', u'', u''' at the cracked region ($x = 0$):

$$u'(0) = \frac{c_1 - c_2}{g} + c_3 \tag{35}$$

$$u''(0) = \frac{c_1 + c_2}{g^2} \tag{36}$$

$$u'''(0) = \frac{c_1 - c_2}{g^3} \tag{37}$$

Substituting Eqs. (1), (21), (22), (35), (36) and (37) into Eq. (26), and after performing some calculations, the material force B is given by
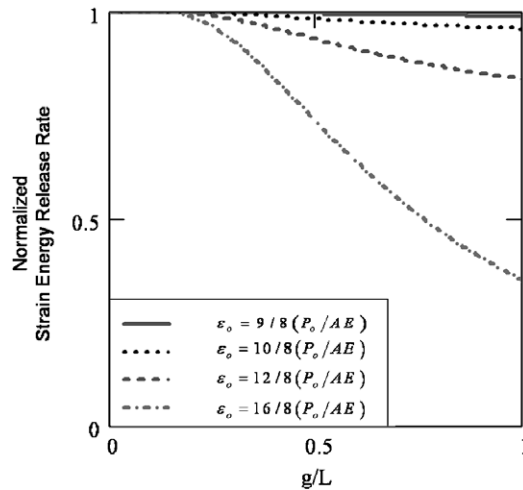
Fig. 7. Dependence of the normalized strain energy release rate, G/G_c of the gradient cracked bar on g/L and for various values of axial strain of the form $\varepsilon_o = f(P_o/AE) \geqslant P_o/AE$.

$$B = -\frac{1}{2}AE\left(c_3^2 + \frac{4c_1c_2}{g^2}\right) \tag{38}$$

Finally, substituting Eqs. (34) and (38) into Eq. (29) one obtains the following expression for the energy release rate G as a jump relation

$$G = \left[\!\left[-\frac{P_o^2}{AE}\left\{\left(1 - \frac{1}{\cosh(L/g)}\right)\left(\frac{AE}{P_o}\varepsilon_o - 1\right)^2\right\}\right]\!\right] \tag{39}$$

Note that Eq. (39) predicts the classical elasticity result, G_c in the limit $g \to 0$

$$G_c = G(g=0) = \left[\!\left[-\frac{P_o^2}{AE}\right]\!\right] = -\frac{P_o^2}{E}\left[\frac{1}{A^*} - \frac{1}{A}\right] \tag{40}$$

Note that if $L \to \infty$, we obtain again the classical result ($g \to 0$). Also note that the term which includes the gradient effects will always make G smaller than G_c (strengthening effect).

Now, the normalized strain energy release rate, G/G_c is plotted in Fig. 7, as a function of the non-dimensional parameter, g/L, and for various values of axial strain of the form $\varepsilon_o = f(P_o/AE) \geqslant P_o/AE$. This plot shows that the normalized strain energy release rate is decreasing monotonically with g/L, predicting a considerably tougher response for the gradient cracked bar, as compared to the classic theory prediction. This deviation becomes very significant for $g/L > 0.25$. Furthermore, the response of the cracked bar is significantly dependent on the value of strain ε_o (for a given value of the parameter g/L, the energy release rate is decreasing for increasing values of ε_o). An interesting scenario could develop if cracks start increasing, leading to increasing ε_o. Eq. (40) could then imply an increasing resistance to crack propagation and increased fatigue life.

4. Conclusions

Based on the strain gradient elasticity framework as particularized on beams and bars, we conclude the followings:

(1) The bending stiffness of the gradient beam as characterized by the deflection and strain metrics has been found to increase with increasing values of the non-dimensional parameter g/L (microstructural length over beam length) as compared to the classical theory prediction.

(2) The characteristic microstructural length g of the present modeling has been assessed for metallic materials. It has been shown that it exhibits a stronger correlation to grain size d as compared to the length calculated with the couple-stress approach.

(3) The maximum tensile strain of the gradient beam has been found to considerably decrease with increasing values of the parameter g/L. This has an apparent implication for the beam's fatigue life. For the present modeling which involves only elastic deformation, the fatigue life approach introduced by Basquin (1910) may be applicable to predict the gradient beam's lifetime. Based on this approach, the reduction of the maximum tensile strain gives a respective decrease in the elastic strain amplitude which implies an increase in the gradient beam's fatigue lifetime.

(4) The toughness of the gradient DCB has been found to considerably decrease with increasing values of the parameter g/L. On the other hand, the toughness of the gradient cracked bar has been found to considerably increase with increasing values of the parameter g/L. These results with reference to two different configurations suggest that, contrary to the common perception, strain gradient theories do not always predict higher strength for small structural components.

Acknowledgements

Appendix A

According to the Koiter theory, the percentage increase $\Delta E/E_o$ of the apparent Young's modulus is given by (Kakunai et al., 1985):

$$\frac{\Delta E}{E_o} = \frac{24(1-v)l^2}{t^2} \tag{A.1}$$

where $v = 0.33$ is the Poisson's ratio, $t = 3.14$ mm is the beam thickness and l is the characteristic length of material. Using these parameters along with the experimentally calculated ratio $l/d = 0.2$ (characteristic length over grain size) into Eq. (A.1), $\Delta E/E_o$ is given by

$$\frac{\Delta E}{E_o} = ad^2 \tag{A.2}$$

where $a = 6.52359 \times 10^{-2}$ mm^{-2} and grain size values d (in mm) used in the experiments, are given in Table 3 of Kakunai et al. (1985).

Now, the normalized deflection u/u_c can be written, in terms of $\Delta E/E_o$, as follows:

$$\frac{u}{u_c} = \frac{E_o}{E} = \frac{E_o}{E_o + \Delta E} = \frac{1}{1 + \frac{\Delta E}{E_o}} \tag{A.3}$$

Substituting Eq. (A.2) into Eq. (A.3) one obtains an expression for the normalized deflection u/u_c as a function of the grain size d.

Finally, using Eq. (8) one obtains the microstructural length g of the current modeling with respect to the grain size d, as shown in Fig. 4.

References

Anderson, W.B., Lakes, R.S., 1994. Size effects due to Cosserat elasticity and surface damage in closed-cell polymethacrylimide foam. J. Mater. Sci. 29, 6413–6419.

Aravas N., 2005. Private communication.

Basquin, O.H., 1910. The exponential law of endurance tests. Proc. ASTM 10, 625–630.

Cosserat, E., Cosserat, F., 1909. Théorie des Corps Déformables. A. Hermann et Fils, Paris.

Eringen, A.C., 1966. Linear theory of micropolar elasticity. J. Math. Mech. 15, 909–923.

Eshelby, J.D., 1975. The elastic energy-momentum tensor. J. Elasticity 5, 321–335.

Georgiadis, H.G., Grentzelou, C.G., 2006. Energy theorems and the *J*-inegral in dipolar gradient elasticity. Int. J. Solids Struct. 43, 5690–5712.

Giannakopoulos, A.E., Amanatidou, E., Aravas, N., 2006. A reciprocity theorem in linear gradient elasticity and the corresponding Saint-Venant principle. Int. J. Solids Struct. 43, 3875–3894.

Kakunai, S., Masaki, J., Kuroda, R., Iwata, K., Nagata, R., 1985. Measurement of apparent Young's modulus in the bending of cantilever beam by heterodyne holographic interferometry. Exp. Mech., 408–412.

Kienzler, R., Herrmann, G., 1986. An elementary theory of defective beams. Acta Mech. 62, 37–46.

Koiter, W.T., 1964. Couple stresses in the theory of elasticity, I & II. In: Proc. K. Ned. Akad. Wet. (B) 67, 17–44.

Lam, D.C.C., Yang, F., Chong, A.C.M., Wang, J., Tong, P., 2003. Experiments and theory in strain gradient elasticity. J. Mech. Phys. Solids 51, 1477–1508.

Mindlin, R.D., 1964. Micro-structure in linear elasticity. Arch. Rat. Mech. Anal. 16, 51–78.

Papargyri-Beskou, S., Tsepoura, K.G., Polyzos, D., Beskos, D.E., 2003. Bending and stability analysis of gradient elastic beams. Int. J. Solids Struct. 40, 385–400.

Rice, J.R., 1968. A path independent integral and the approximate analysis of strain concentration by notches and cracks. ASME J. Appl. Mech. 35, 379–386.

Senturia, S.D., 2001. Microsystem Design. Kluwer Academic Publishers, Boston.

Tsepoura, K.G., Papargyri-Beskou, S., Polyzos, D., Beskos, D.E., 2002. Static and dynamic analysis of a gradient elastic bar in tension. Arch. Appl. Mech. 72, 483–497.

Vardoulakis, I., Sulem, J., 1995. Bifurcation Analysis in Geomechanics. Blackie/Chapman and Hall, London.

Yang, J.F.C., Lakes, R.S., 1982. Experimental study of micropolar and couple stress elasticity in compact bone in bending. J. Biomech. 18 (2), 91–98.